Density functional study of structure and dynamics in liquid antimony and Sb_n clusters

R. O. Jones, O. Ahlstedt, J. Akola, and M. Ropo

Citation: The Journal of Chemical Physics **146**, 194502 (2017); doi: 10.1063/1.4983219
View online: http://dx.doi.org/10.1063/1.4983219
View Table of Contents: http://aip.scitation.org/toc/jcp/146/19
Published by the American Institute of Physics

Density functional study of structure and dynamics in liquid antimony and Sb_n clusters

R. O. Jones,[1,a)] O. Ahlstedt,[2] J. Akola,[2,3] and M. Ropo[2,4]
[1]*Peter Grünberg Institut PGI-1 and JARA/HPC, Forschungszentrum Jülich, D-52425 Jülich, Germany*
[2]*Laboratory of Physics, Tampere University of Technology, P.O. Box 692, FI-33101 Tampere, Finland*
[3]*Department of Physics, Norwegian University of Science and Technology, NO-7491 Trondheim, Norway*
[4]*COMP Centre of Excellence, Department of Applied Physics, Aalto University, FI-00076 Aalto, Finland*

(Received 7 February 2017; accepted 27 April 2017; published online 18 May 2017)

Density functional/molecular dynamics simulations have been performed on liquid antimony (588 atoms and six temperatures between 600 K and 1300 K) and on neutral Sb clusters with up to 14 atoms. We study structural patterns (coordination numbers, bond angles, and ring patterns, structure factors, pair distribution functions) and dynamical properties (vibration frequencies, diffusion constants, power spectra, dynamical structure factors, viscosity) and compare with available experimental results and with the results of our previous simulations on Bi. Three short covalent bonds characteristic of pnictogens are common in the clusters, and higher temperatures lead in the liquid to broader bond angle distributions, larger total cavity volumes, and weaker correlations between neighboring bond lengths. There are clear similarities between the properties of Sb and Bi aggregates. *Published by AIP Publishing.* [http://dx.doi.org/10.1063/1.4983219]

I. INTRODUCTION

The structures and other properties of group 15 elements (pnictogens, valence configuration ns^2np^3) have aroused interest for many years.[1] The heavier members of the group (P, As, Sb, and Bi) have numerous crystalline forms, most showing a preference for threefold coordination and bond angles near 60° and 90°. The $A7$ structure (rhombohedral, $R\bar{3}m$, D^5_{3d}) is the most stable (α-)form of the semimetals As, Sb, and Bi. It comprises puckered layers of atoms with bonds of equal length r_ℓ to three neighbors, as well as bonds of length r_d to three atoms in the next layer. Table I shows that the ratio r_d/r_ℓ decreases with increasing atomic number, which is similar to the effect also found in group 16 elements (S, Se, Te, Po) for the ratio of "interchain" to "intrachain" distances.[6,7] Apart from a scaling factor, the structures of Sb and Bi are remarkably similar. In phosphorus, the black (orthorhombic) allotrope can be converted under pressure to the $A7$ structure and—at much higher pressures—to a simple cubic metallic form.[2] Elements P to Bi can all be made superconducting by the application of pressure,[8] which usually results in a structural phase change.

Group 15 elements also play an important role in the rapidly growing field of topological phase transitions, where gapless surface or edge states are protected against perturbations that do not close the band gap. Topologically protected spin states could possibly lead to interesting electronic devices, and studies of layer structures related to the $A7$ bulk structure of group 15 elements include work on black P layers (phosphorene),[9] As monolayers,[10] layered crystalline (antimonene) phases,[11] the Sb(111) surface,[12] and a Bi(111) bilayer.[13]

A variety of structural patterns and other properties have made group 15 elements attractive objects of study for many years,[14–16] and unusual features in the $P-T$ phase diagrams include liquid-liquid phase transitions at high T and P.[17–22] High pressures suppress the simple cubic to $A7$ transition in P, As, and Sb,[23] and inelastic neutron scattering (INS) measurements of the dynamical structure factor $S(q,\omega)$ near the melting point of Bi show evidence of collective density excitations.[24–26] In liquid Sb, both the change in the slope of the temperature dependence of the electrical resistivity $\rho(T)$ around 1000 K[27] and the unusual maximum in the sound velocity at 1168 K[28–30] suggest structural changes, and neutron scattering studies of the static structure factor and pair distribution function have been carried out.[22,31] Liquid Sb is a favored component of the positive electrode in liquid metal batteries being developed for grid-level energy storage.[32]

Simulations of liquid pnictogens include tight-binding Monte Carlo studies of As and Sb by Bichara *et al.*[33] and on Sb and Bi by Hafner and Jank,[34] who performed molecular dynamics on samples with up to 2000 atoms using an effective pair potential. DF/MD simulations of liquid As were carried out by Li (64 atoms, 1150 K, 0.3 ps after equilibration),[35] and the first such simulation of liquid Sb was performed by Seifert *et al.*,[36] on a 64-atom sample over 8.1 ps at 1073 K. The crystallization of liquid Sb in the presence of crystalline Sb templates was studied in 144 atom samples at 600 K.[37]

In 1934, Jones[38,39] explained the high diamagnetism, low (semimetallic) conductivity, and structure of bismuth as a distortion of a simple cubic structure brought about by the existence of a large (Jones) zone containing five valence electrons per atom. This work provides a natural explanation of the $A7$ crystalline structure of As, Sb, and Bi but has largely been overlooked. Peierls[40] discussed the same mechanism in one dimension more than 20 years later, and the "Peierls

a)Electronic mail: r.jones@fz-juelich.de

TABLE I. *A*7 crystal structure ($R\bar{3}m$, D^5_{3d}) of group 15 elements at room temperature: high-pressure P, α-As, α-Sb, α-Bi, intralayer bond length r_ℓ, interlayer separation r_d, intralayer bond angle (α_0).

	P[a]	α-As[b]	α-Sb[c]	α-Bi[d]
r_ℓ (Å)	2.13	2.517	2.908	3.072
r_d (Å)	3.27	3.120	3.355	3.529
r_d/r_ℓ	1.535	1.240	1.154	1.149
α_0 (deg)	105.0	96.6	95.6	95.5

[a]Reference 2.
[b]Reference 3.
[c]Reference 4.
[d]Reference 5.

distortion"[41] has often been invoked in discussions of the structures of group 15 liquids, all of which are characterized by a short-range order similar to that of the *A*7 structure.[42] An analysis of the pair distribution function [PDF, $g(r)$] in liquid P, As, Sb, and Bi[42] indicated that such a distortion is present in all cases and appears to increase with increasing temperature due to the larger volume available.[42] On the other hand, X-ray absorption fine structure (XAFS) spectroscopy indicates that a Peierls distortion is weak in liquid Sb near the melting point and vanishes around 1000 K as the temperature increases.[43]

Antimony cluster cations Sb_n^+ have been identified mass spectroscopically to $n > 250$.[44–46] There is a clear preference for n to be a multiple of 4, which has been explained by a model of packed Sb_4 tetrahedra.[44] Photoelectron spectra have been determined for Sb_2^+ and Sb_4^+ (Ref. 47) and for the anions Sb_n^- for $n = 1$–4[48] and $n = 2$–9.[49] Laser induced fluorescence provides the most detailed information about Sb_2,[50] Raman spectra of the dimer and tetramer have been measured in neon matrices,[51] and the equilibrium dissociation energies of Sb_2, Sb_3, and Sb_4 have been measured in the gas phase.[52] Calculations using correlated wave functions have been performed on Sb_2,[53,54] Sb_3,[55,56] and Sb_4,[57] but DF methods have been favored for larger clusters. They include Sb_n^- ($n = 2$–9),[49] Sb_n ($n = 2$–8, 12),[58] and Sb_n ($n = 2$–10).[59]

The structures of group 15 elements have been studied in our group for many years. Clusters of phosphorus were among the first where unexpected structures were found using simulated annealing,[60,61] and calculations on clusters of P and As[62] showed that improved cohesive energies resulted when a gradient corrected form[63] of the exchange-correlation energy was used. The polymerization of a liquid comprising P_4 molecules to a disordered network[64] was one of the first phase transitions simulated using density functional (DF)[65] molecular dynamics (MD) methods. Ballone and Jones[66] studied the liquid-liquid phase transition in a 4000-atom sample of P using a classical force field with parameters fit to an extensive set of DF calculations on phosphorus clusters. Most recently, we performed DF/MD simulations on liquid Bi at four temperatures between 573 K and 1023 K.[67,68] These simulations provided much information on the structure and dynamics of liquid Bi, including collective excitations, and also of Bi_n clusters with $n \leq 14$.[67]

We present here the results of DF calculations of the structures and energies of Sb_n clusters up to $n = 14$ and compare where possible with other calculations (DF and correlated wave functions) and with the experiment. We also describe extensive DF/MD simulations of liquid Sb (melting point 903.8 K) at six temperatures between 600 K and 1300 K. The latter forms a part of a continuing study of the rapid crystallization of liquid Sb.[69] We study structural patterns (coordination numbers, bond angles, and ring statistics), structure factors, pair distribution functions, and dynamical properties (vibration frequencies, diffusion constants, power spectra, dynamical structure factors, viscosity) and compare with available experimental results and the results of our Bi simulations. We comment on the evidence for Peierls distortions at different temperatures and the limitations of the approximate exchange-correlation energy functionals used in our calculations.

II. METHODS OF CALCULATION

A. Density functional calculations

The calculations were performed with the CPMD program[70] using Born-Oppenheimer MD, periodic boundary conditions with a single point ($\mathbf{k} = 0$) in the Brillouin zone, and scalar-relativistic (s-r) Troullier-Martins[71] pseudopotentials (PP) with five valence electrons ($5s^25p^3$) and a 20 Ry cutoff. The exchange-correlation functional of Perdew, Burke, and Ernzerhof (PBE)[72] was used, and non-linear core corrections were included.[73] The effect of spin-orbit coupling on the relative energies of cluster isomers is weak and is discussed in Sec. IV D. For the liquid samples (588 atoms), we used the PBEsol approximation,[74] and the density cutoff for calculating the gradient corrections was 1.0×10^{-5} in all cases. Optimization of the *A*7 crystal structure using this functional gave $r_l = 2.924$ Å, $r_d = 3.547$ Å, $\alpha_0 = 98.4°$, compared with the experimental values (Table I) 2.908 Å, 3.355 Å, and 95.6°. While the interlayer bond lengths are described well, the separation *between* layers is overestimated by over 5%. Similar discrepancies arose when applying the PBE functional to Te, the neighbor of Sb in the periodic table.[6] However, better results—with substantially higher computational cost—were obtained in liquid Te (Ref. 6) using the approximation of Tao *et al.*[75] and in liquid tellurides[76] using an empirical correction for dispersion forces.[77] These results indicate that improved functionals are needed for high precision calculations, without implying that these particular modifications (TPSS, dispersion corrections) are individually essential.

Liquid Sb was simulated at six temperatures in hexagonal simulation boxes with parameters given in Table II. The hexagonal symmetry is compatible with that of bulk Sb, as the results formed a part of a continuing study of crystallization of liquid Sb.[69] The densities at the melting point and above were taken from Ref. 78, and those of supercooled samples were assumed to be the same as at 900 K. The time step was 3.025 fs. The simulations proceeded by successive cooling of the liquid structure found at 1300 K, with adjustments to the size of the cell if required. Equilibration was performed over 10 ps at each temperature before data collection (coordinates r_i and velocities v_i of all atoms) over the simulation times given in Table II. The long simulation at 600 K was a part of the crystallization study mentioned above.

TABLE II. Parameters for the hexagonal simulation cell. The number of atoms (588) and the *c*/*a* ratio (0.738) are the same in all cases.

T (K)	a (Å)	At. dens. (Å^{-3})	Data coll. (ps)
600	30.6390	0.0320	574
700	30.6390	0.0320	108
900	30.6390	0.0320	101
1000	30.7370	0.0317	101
1100	30.8349	0.0314	101
1300	31.0344	0.0308	101

Excellent starting structures for the calculations of Sb_n isomers could be found in most cases by scaling the coordinates of structures found for Bi_n,[67] many of which had been found in turn for $n \leq 10$ by scaling the coordinates of low-lying structures of P_n[60,61] and locating the nearest energy minimum. Larger cluster structures were generated by adding atoms to edges or faces of stable clusters or by combining pairs of clusters. States with the lowest possible multiplicity are generally the most stable, but higher multiplicity states have been checked in most structures with $n < 10$.

B. Analysis of results

The pair distribution function (PDF) $g(r)$ is the spherically averaged distribution of interatomic vectors $(r_j - r_i)$ and can be determined from the atomic coordinates

$$g(r) = \frac{1}{\rho^2}\left\langle \sum_i \sum_{j\neq i} \delta(r_i)\delta(r_j - r)\right\rangle , \quad (1)$$

where ρ is the atomic number density. The structure factor $S(q)$ is the Fourier transformation of $g(r)$,

$$S(q) = 1 + \rho \int_0^\infty dr\, 4\pi r^2\, [g(r) - 1]\, \frac{\sin(qr)}{qr}. \quad (2)$$

The local structure is also characterized by the distributions of the bond angles, the near-neighbor separations, and the ring structures.[79] Cavities were calculated using the pyMolDyn program[80] with cutoff radius 2.8 Å.

The frequency distributions (power spectra) of the liquid phases have been calculated from the velocity-velocity autocorrelation function Cv,

$$C_v(t) = \frac{1}{N}\sum_{i=1}^{N} \frac{\langle v_i(t_0)\cdot v_i(t)\rangle}{\langle v_i(t_0)\cdot v_i(t_0)\rangle}, \quad (3)$$

which was evaluated in a given trajectory for blocks of 20 000 time steps (over 60 ps) with different starting points t_0. The Fourier transform of the average then gives the power spectrum. Cluster vibration frequencies were calculated by diagonalizing the dynamical matrix, whose elements are found using finite differences. Calculations using linear response theory gave results that were typically 1%–2% lower. Vibration frequencies were broadened by a Gaussian of width 1 cm^{-1}. The diffusion constants D were calculated from the coordinates r_i,

$$D = \lim_{t\to\infty} \frac{\left\langle |r_i(t) - r_i(0)|^2\right\rangle}{6t}. \quad (4)$$

The dynamical structure factor $S(q,\omega)$ is determined from the current autocorrelation functions as described in detail in Ref. 68. The shear viscosity η couples to the transverse momentum and can be calculated from the transverse current autocorrelation function and its Laplace transform. Extrapolation to $q = 0$ is carried out using an equation suggested by Alley and Alder based on a hydrodynamic model[81]

$$\eta(q) = \frac{\eta}{1 + a^2q^2}\ , \quad (5)$$

where η is the shear viscosity and a is an adjustable parameter. Full details are provided in Ref. 68.

A simple connection between viscosity η and diffusion constant or diffusivity D is the Stokes-Einstein relationship (SER)[82,83] derived for the diffusion of uncorrelated macroscopic spheres in a liquid,

$$D(T)\eta(T) = \frac{k_BT}{c\pi d}\ , \quad (6)$$

where d is an effective diameter of a sphere, and c is a constant that depends on the boundary conditions between the particle and fluid (slip: $c = 2$, stick: $c = 3$). The SER can be applied to the diffusion of single atoms or molecules at high temperatures and for predictions if one of these quantities is unknown.

III. LIQUID ANTIMONY

A. Structure factor, pair distribution function, and near-neighbor separations

A representative snapshot of the liquid at 900 K is shown in Fig. 1, and in Fig. 2 we show the PDF and structure factors $S(q)$ for the liquid at 900 K, 1000 K, 1100 K, and 1300 K. Also shown are the experimental (ND) results of Greenberg *et al.*[30] Although the temperatures of the two sets of data are not identical, the agreement between theory and experiment is encouraging. The calculations reproduce the main features of the experiments very well, including the existence of a weak shoulder in $S(q)$ on the high-q side of the first peak. Nevertheless, the details of this shoulder are less satisfactory, particularly at 900 K. We note that the experimental data for 923 K are slightly less precise than those at the other three temperatures, for which the background scattering was determined directly without interpolation.[84]

The distribution of separations of up to the 12 nearest neighbors [Fig. 3] shows interesting features. While bonds to the more distant neighbors expand steadily as the temperature increases, there is little change in the distance to the first three neighbors. The maxima of the nearest-neighbor distributions at all temperatures (~2.83 Å) are slightly shorter than the

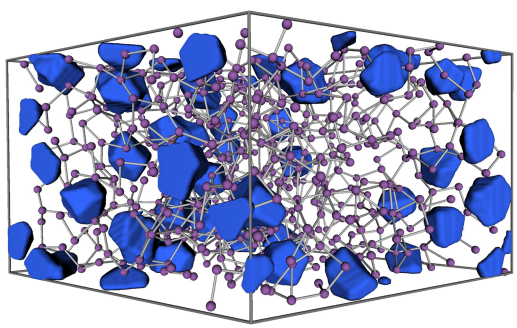

FIG. 1. Snapshot of liquid Sb at 900 K. Cavities are shown in blue.

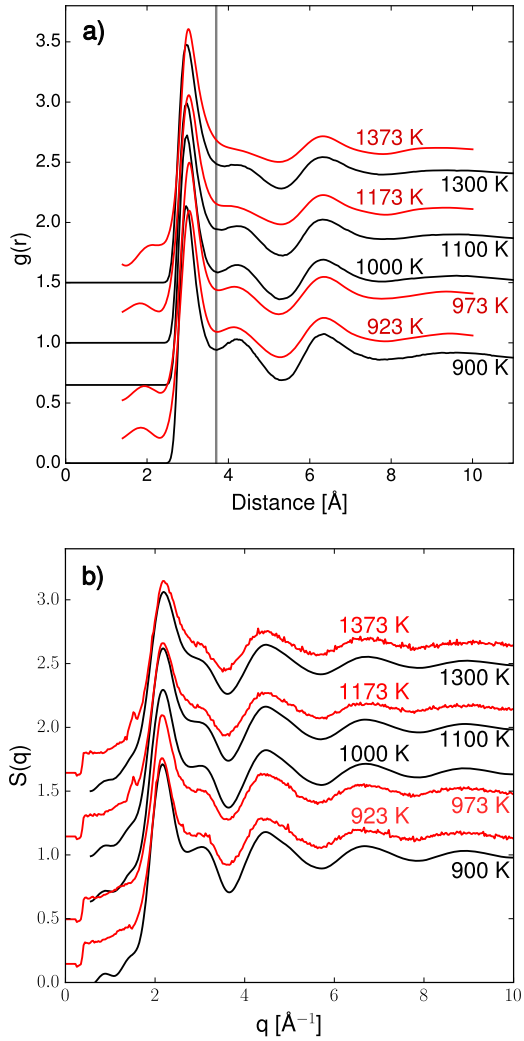

FIG. 2. (a) Pair distribution functions for liquid Sb at the temperatures shown. Black: present calculations and red: neutron scattering data (Ref. 30). The vertical line is for distance 3.7 Å. (b) Corresponding structure factors. Curves are offset to improve clarity and reflect the different temperatures.

nearest-neighbor separation in crystalline Sb (2.908 Å). Distributions 4–6 are still below 3.7 Å and show a smaller shift and narrower distributions than more distant neighbors (7–12), which is reminiscent of the situation in Bi.

To avoid ambiguities arising from the relatively broad first peak in the PDF, we have employed the effective coordination number ECN,[85] where the average value of bond distances is calculated iteratively for each atom and the bonds are weighted accordingly. The calculated ECN-values at 600, 700, 900, 1000, 1100, and 1300 K are 4.87, 5.13, 5.31, 5.26, 5.19, and 5.05, respectively. To reproduce these values by integrating $g(r)$, the corresponding cutoff distances are 3.13, 3.21, 3.27, 3.29, 3.23, and 3.20 Å. The overall picture is approximately fivefold coordination with a weak maximum near the melting point.

B. Bond angle distributions

The bond angle distributions [Fig. 4] were determined with a cutoff of 3.0 Å, which means that long bonds are excluded, and they show a preference for octahedral orientation at lower temperatures (bond angles around 90° and nearly

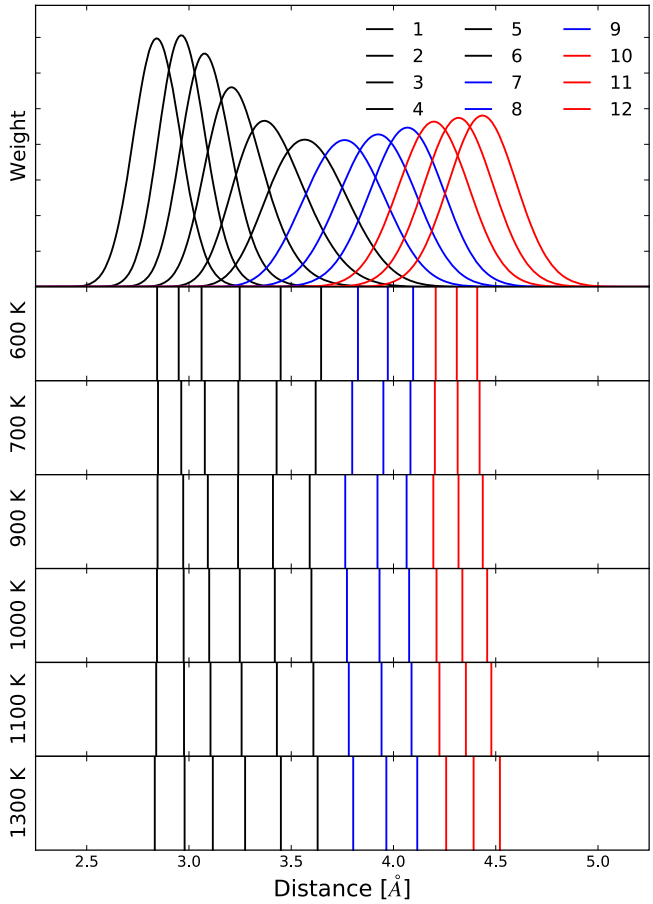

FIG. 3. Near-neighbor distributions in liquid Sb at 600 K. Below are shown the average distances of each neighbor at all simulation temperatures.

linear configurations). The distributions become weaker and broader as the temperature is increased, while triangular configurations (~60°) become more important. The bond angle distributions are discussed further in Sec. V.

C. Rings and cavities

Rings and cavities are analyzed as described above (Sec. II B). Simulations of hundreds of atoms are needed to avoid distortions caused by periodic boundary conditions.

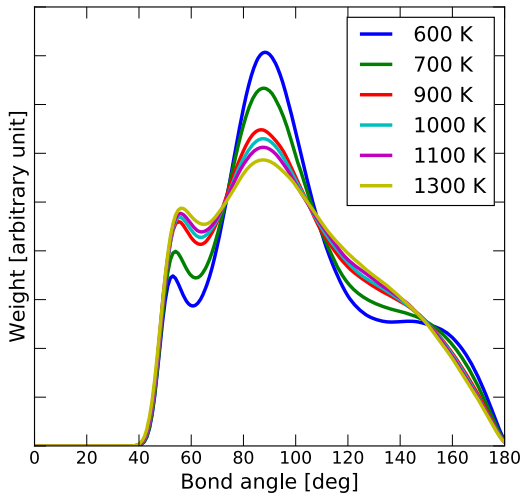

FIG. 4. Bond angle distributions at all temperatures.

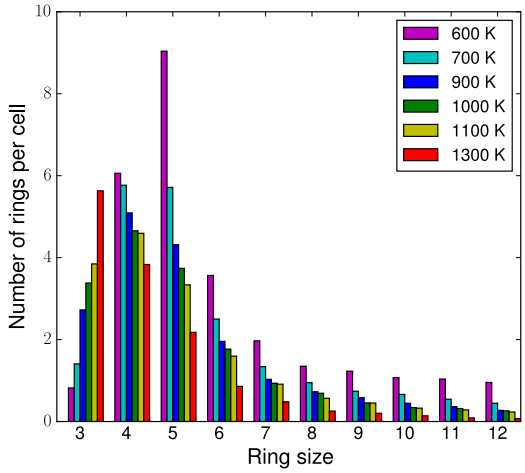

FIG. 5. Ring distributions in liquid Sb at six temperatures.

The distribution of rings (closed paths along bonds) is shown in Fig. 5 for all six temperatures (cutoff 3.0 Å). Rings with three or four atoms are common, and there is more weight for larger rings at a higher temperature. These changes reflect the reduced coordination and atomic density at high T. The supercooled sample at 600 K shows an increased weight of five- and six-fold rings. The latter become the main structural motif in crystalline Sb and are likely to play an important role in the crystallization of the liquid.[86]

Cavity analysis was performed with the pyMolDyn program[80] using a sphere radius of 2.8 Å. The differences between the temperatures are significant, but less pronounced than in Bi. The total cavity volumes increase from 3.9% at 600 K to 10.1% at 1300 K, consistent with the lower densities measured at higher temperatures.[78] As in liquid Bi, this change is reflected in the shift of the near-neighbor distributions 7–12 (Fig. 3), corresponding to distances on the second coordination shell.

D. Vibrations, diffusion

The power spectra (vibrational densities of states) are shown in Fig. 6 for liquid Sb at all six temperatures. There is a broad peak at 12–16 meV that moves to lower frequencies as the temperature is increased. These frequencies are in the range found in optical phonons in crystalline Sb[87] and a second peak (~2 meV) at 600 and 700 K. The tail of the distribution above ~18 meV arises from bond stretching modes that are also apparent in Sb_n clusters (see Sec. IV C).

We have used the TwoPT program[88] to separate the power spectra into contributions from diffusive (gaslike, g) and vibrational (solid, s) modes. The result is shown in Fig. 7. This program allows us to determine the value of the diffusion constant, and the results (D_{sg}) show very good agreement with values D calculated from Eq. (4) (see Table III). Diffusion constants measured by radioactive tracer diffusion in liquid Sb are (units of 10^{-5} cm^2/s) 5.81 ± 0.47 at 955 K, 6.46 ± 0.55 at 1001 K, 8.68 ± 1.17 at 1185 K, and 10.95 ± 0.68 at 1302 K.[89] Our results agree well at 1300 K and somewhat underestimate the measured values at lower temperatures, although the error bars in the latter are substantial.

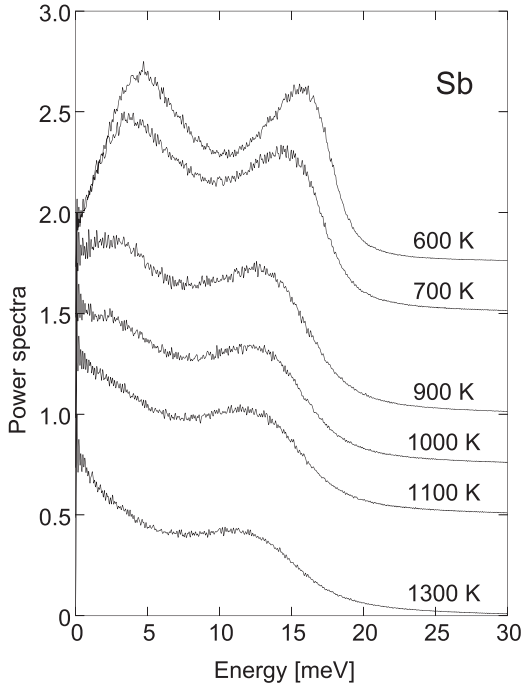

FIG. 6. Calculated power spectra for liquid Sb at six temperatures. Each curve has its maximum value at unity.

E. Dynamical structure factor, collective dynamics

The dynamical structure factors $S(q, \omega)$ for selected q values were calculated from the MD trajectories at 600–1300 K, and the ratios to the static structure factors $S(q)$ are given in Fig. SF1 of the supplementary material for selected values of q. We show results obtained directly from the trajectories as well as those using a Gaussian window function ($\sigma = 3$ meV) to reduce numerical noise.

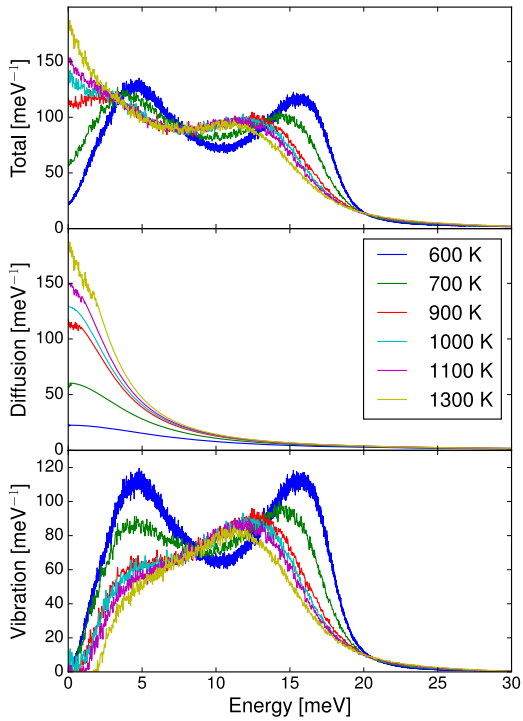

FIG. 7. Power spectra (states per meV) for liquid Sb, separated into diffusive (gaslike) and vibrational (solid-like) modes.

TABLE III. Self-diffusion constants (10^{-5} cm^2/s) of Sb at temperatures T (K). D: calculated from trajectory using Eq. (4) and D_{sg}: calculated using TwoPT program (Ref. 88). Also shown are sound velocities c (m/s) and shear viscosities η (mPa s).

T	600	700	900	1000	1100	1300
D	0.525	1.514	4.106	5.160	6.665	10.459
D_{sg}	0.542	1.696	4.244	5.176	6.621	10.257
c	2520	2464	2506	2460	2461	2312
η			1.53	1.09	0.99	0.74
η (expt.)[a]			1.43	1.19	1.03	0.81

[a]Reference 78.

The dispersion relations obtained from the peaks of the longitudinal current correlation function $C_L(q,\omega)$ are shown for $T = 900$ K in Fig. 8. For a given value of q, $C_L(q,\omega)$ can have more than one maximum, and care is needed in identifying the collective modes. We show the results for all values of q (red crosses), as well as those using bins in q of width 0.1 Å^{-1}. The results can be summarized as follows. A linear relationship between ω and q for the diffusive single-particle modes below 0.6 Å^{-1} is followed by a relatively flat dispersionless range between 0.7 and 1.6 Å^{-1}. This behavior is very similar to that found in Bi.[68] As in Bi, there is a deep minimum near $q = 2.0$ Å, which is close to the reciprocal lattice vector where a minimum occurs in the phonon spectrum of crystalline Bi.[87] A

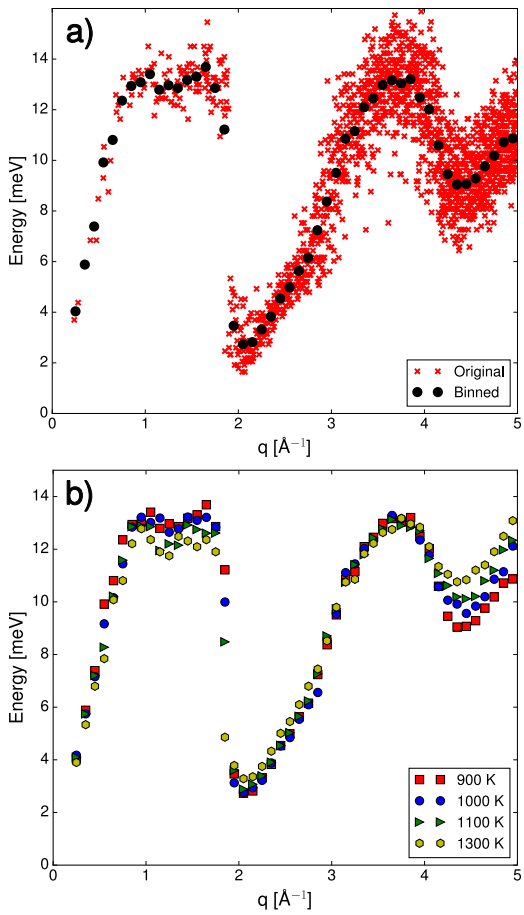

FIG. 8. (a) Longitudinal dispersion curves at 900 K. Red crosses: calculation and black circles: results using q-bins of width 0.1 Å^{-1}. (b) Longitudinal dispersion curves for liquid Sb (binned) at the temperatures given.

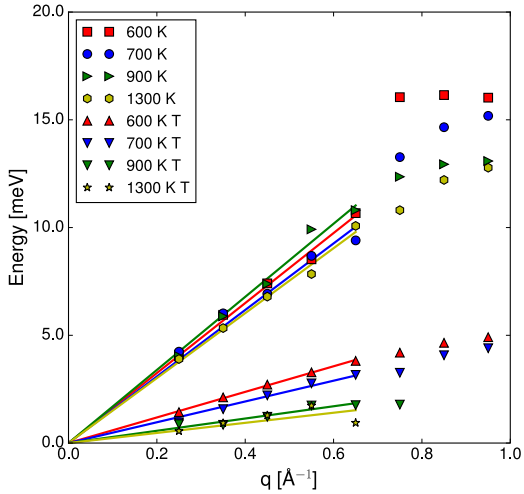

FIG. 9. Dispersion of longitudinal (upper curves) and transverse (lower curves) modes at 900, 1000, 1100, and 1300 K.

second, weaker minimum occurs at approximately twice this wave vector.

The dispersion curves for low values of q are shown in Fig. 9 for four temperatures. The sound velocities can be calculated from the linear part of the dispersion curves, and linear fits to the low q values are shown in Fig. 9 as solid lines. The sound velocities c calculated in this way depend on the number of fitting points and how the data are averaged. Taking the origin and q-points up to 0.5 Å, we find a sound velocity at 900 K of 2506 m/s, compared with experimental values at the melting point (903.8 K, 1910,[28,90] 1884 m/s[29]). The values at all temperatures are given in Table III. The low-frequency (hydrodynamic) value of the sound velocity is then over 20% lower than the sound velocity determined here. This effect is known as "positive dispersion" and was also observed in Bi.[68] Our fitting procedure leads to considerable uncertainties in the results, but a maximum in the sound velocity a little above the melting point remains a possibility.

Side peaks in the calculated $C_T(q,\omega)$ spectra provide information about the transverse modes. They have been analyzed as in the case of Bi[68] and are again much weaker than peaks in the corresponding $C_L(q,\omega)$. The sound velocities for the transverse modes are 900 (600 K), 730 (700 K), 430 (900 K), and 360 m/s (1300 K).

F. Viscosity

The calculation of the q-dependent shear viscosity from the transverse current correlation function is discussed in Ref. 68. This function is then extrapolated to the limit $q \to 0$ using Eq. (5), and the results are shown for four temperatures in Fig. 10. The calculated shear viscosities are compared with experimental values[78] in Table III. The extrapolated value depends on the choice of q-points as well as the fit function (5). We have chosen a cutoff of 3.0 Å^{-1} and points in the tail of $\eta(q)$ separated by 0.2 Å^{-1}. In view of these uncertainties, the agreement with the experiment is satisfactory. At lower temperatures, $\eta(q)$ increases rapidly as $q \longrightarrow 0$. Since the lowest q value is fixed by the size of the simulation cell at ~0.24 Å^{-1}, the extrapolation is no longer reliable.

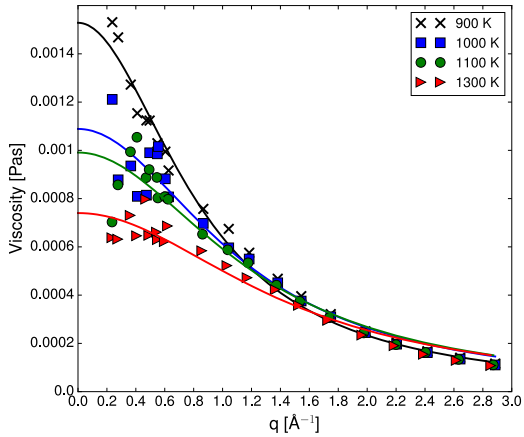

FIG. 10. Viscosity calculated from transverse current correlation function for 900, 100, 100, 1300 K. Crosses: calculated values and lines: fits using Eq. (5) to estimate viscosity at $q = 0$.

The Stokes-Einstein relationship [Eq. (6)] between viscosity η and diffusion constant D was derived for a very simple model, but it is often satisfied fairly well (within ~20%) for monatomic liquids. If we assume that the diameter d of an Sb sphere corresponds to the first peak in the pair distribution function (3.0 Å for all temperatures) and adopt the values of D determined by the TwoPT program (Table III), we find the following values of η using the SER: 900 K: 1.63, 1000 K: 1.42, 1100 K: 1.21, 1300 K: 0.77 [$10^{-5}\times$ cm^2/s], somewhat higher than the measured values of η given above.

G. Electronic structure

The general features of the electronic band structure of crystalline Sb are well known.[91] The three bands near the Fermi energy arising from atomic 6*p*-electrons have antibonding, lone-pair, and bonding components and are separated by ~4 eV from two bands at lower energies arising from the 6*s*-electrons. The Kohn-Sham eigenvalue spectra (electronic density of states, DOS) for 600, 900, and 1300 K are shown in Fig. 11. Also shown are the results for a crystalline sample with the density at 900 K (6.466 g cm^{-1}), which is 3.5% lower than the density at 300 K. The overall picture shows two broad bands

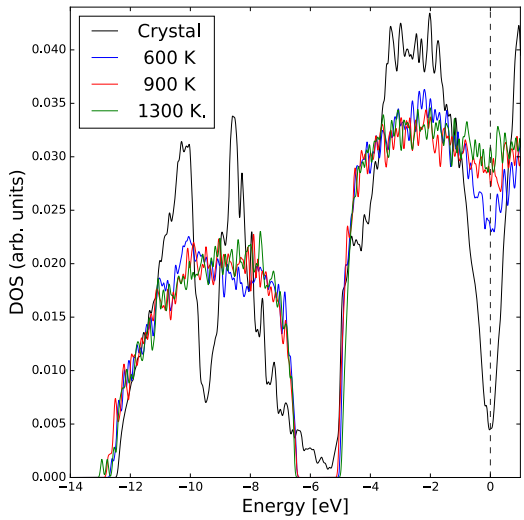

FIG. 11. Electronic density of states for crystalline Sb and for liquid Sb at 600, 900, and 1300 K. The Fermi energy is zero in each case.

from the Fermi energy to −5 eV and between −7 and −13 eV. The density of states shows a very pronounced minimum at the Fermi energy, which is consistent with its semimetallic nature, but this minimum is weak or non-existent at the melting point and above.

IV. ANTIMONY CLUSTERS Sb$_n$

Structures, energies, and vibration frequencies have been calculated as described in Sec. II A for isomers of Sb$_n$ clusters up to $n = 14$.

A. Structures

Results of calculations for the dimer Sb$_2$ are compared with the experiment in Table IV. The DF calculations lead to a consistent picture of bond lengths, and the differences in the binding energies reflect in part the use of different approximations for the exchange-correlation energy.

The Sb trimer has two low-lying isosceles triangular (C_{2v}) isomers that are Jahn-Teller distortions of the equilateral triangle structure (D_{3h}). The $^2A_2$ state ($\alpha = 64.2°$, $r_1 = 2.73$ Å, $r_2 = 2.90$ Å) is slightly (0.02 eV) more stable than the $^2B_1$ state ($\alpha = 56.1°$, $r_1 = 2.84$ Å, $r_2 = 2.67$ Å). Similar structures and the same ordering were found in the multireference configuration interaction (MRCI) calculations of Balasubramanian *et al.*[55] ($^2A_2$, 65.8°, $r_1 = 2.76$ Å; $^2B_1$, $\alpha = 55.6°$, $r_1 = 2.90$ Å, $\Delta E = 0.04$ eV) and the CCSD(T) calculations of Choi *et al.*,[56] ($^2A_2$, $\alpha = 64.2°$, $r_1 = 2.73$ Å; $^2B_1$, $\alpha = 56.2°$, $r_1 = 2.84$ Å, $\Delta E = -0.05$ eV). The linear structure ($r = 2.58$ Å) lies 1.74 eV above the $^2A_2$ state and has vibration frequencies 29, 168, and 247 cm^{-1}. The most stable tetramer is tetrahedral (T_d, bond length 2.86 Å). The C_{2v} (butterfly) structure of Sb$_4$ is a familiar unit in clusters of P and As and lies 1.40 eV higher in energy than the T_d structure. There are four bonds of length 2.84 Å and one of 2.90 Å.

Two low-lying stable isomers of each of Sb$_5$, Sb$_6$, and Sb$_7$ are shown in Fig. SF2 (supplementary material). The stability of the structures comprising the butterfly tetramer with an additional atom [5(a)], dimer [6(b)], and trimer [7(a)] is evident. With the exception of the twofold coordinated dimer atoms (2.65 Å), the bond lengths in these structures lie in a

TABLE IV. Spectroscopic constants of Sb$_2$. R-CI: relativistic configuration interaction and DF: density functional.

	r_e (Å)	ω_e (cm^{-1})	E_B (eV)
R-CI[a]	2.58	259	2.17
R-CI[b]	2.578	240	
DF[c]	2.55	276	3.18
DF[d]	2.51	273	3.07
Expt.[e]		269.25	
Expt.[f]		270.4	
Expt.[g]	2.476	269.623	3.11[h]

[a]Reference 53.
[b]Reference 54.
[c]Reference 59.
[d]This work.
[e]Reference 48.
[f]Reference 51.
[g]Reference 50.
[h]Reference 52.

narrow range (2.84–2.90 Å). The longest bonds occur in the C_{4v} isomer of Sb_5 (2.90 Å, 2.95 Å), where the out-of-plane atom is fourfold coordinated. As in the case of Bi_7, the energies of 7(a) and 7(b) are almost degenerate.

Low-lying isomers of Sb_8 are shown in Fig. SF3 (supplementary material), and the wedge (C_{2v}) structure is the most stable. Of particular interest is the relative stability of a pair of Sb_4 tetrahedra, where there are numerous local minima in the energy surface. The most stable [0.09 eV above (a)] is found when faces of the two tetrahedra (bond lengths 2.86 Å) are nearly parallel [8(b)]. The distance between atoms in different tetrahedra is 4.2 Å, and the bonds in the tetrahedra are 2.87 Å. Slightly higher in energy is isomer 8(c), which has a mirror plane and shorter bonds (3.99 Å) between the tetrahedra. The PBE and similar approximations usually overestimate the strengths of weak bonds between closed shell systems, but the results demonstrate the importance of "clusters of clusters" in group 15 elements. Isomers 8(g) (D_{2h}, with all bonds close to 2.87 Å) and 8(h) (O_h, cube, bond length 2.93 Å) of Sb_8 lie 0.43 eV and 0.67 eV, respectively, above the most stable isomer.

Two low-lying isomers of each of Sb_9 to Sb_{14} are shown in Figs. SF4 and SF5 in the supplementary material. Many structures can be derived from smaller clusters by adding units with one to four atoms, and structures with higher symmetry, e.g., C_{2h} in Sb_{10}, Sb_{11}, and Sb_{12}, are favored over their lower symmetry counterparts (C_s). The structures found in larger clusters indicate a preferred direction of growth reminiscent of tube-like structures found in monoclinic phosphorus.[1] Further remarks on bonding trends are given in Sec. IV D.

B. Cohesive energies

In Fig. 12 we show the calculated binding energies per atom (cohesive energy E_c), as well as the DF results of Ref. 59.

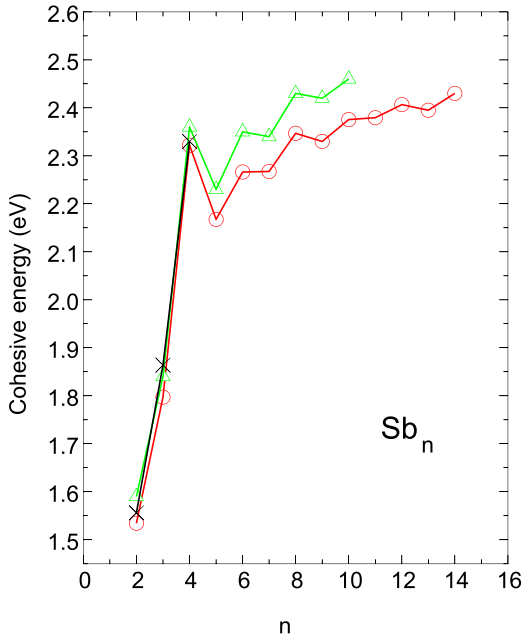

FIG. 12. Cohesive energies of Sb_n clusters. Present work: red circles, DF calculations (Ref. 59): green triangles, experiment (Sb_2, Sb_3, Sb_4, Ref. 52): black crosses. The measured cohesive energy of bulk Sb is 2.74 eV/atom (Ref. 92).

The variation of E_c with the cluster size follows the pattern found in phosphorus clusters: a general increase with a clear odd-even alternation, and there is reasonable agreement between the two sets of results. Experimental values for Sb_2, Sb_3, and Sb_4[52] agree well with our calculations. The measured enthalpy of vaporization in bulk Sb is 2.74 ± 0.02 eV.[92] The relatively slow variation of E_c with $n \geq 6$ indicates that assemblies of small clusters, such as isomer 8(b), can have similar energies to more compact clusters with the same total number of atoms.

C. Vibration frequencies

Vibration frequencies for representative isomers of Sb_n clusters are shown in Fig. SF6 (supplementary material). Previous vibration frequency calculations for Sb_n clusters with $n > 2$ appear to be limited to the trimer.[56] While the results depend on the choice of the basis set and effective core potential, the results compare reasonably well with ours. In the $^2A_2$ state, the present calculations give 114, 152, and 230 cm^{-1}, compared with 149 and 229 cm^{-1} with CCSD(T) calculations.[56] Our calculations for linear Sb_3 give frequencies of 134, 174 (3), and 234 cm^{-1} (2). With the exception of Sb_2, there are few measurements of vibration frequencies in Sb_n clusters. Bondybey, Schwartz, and Griffiths[51] found 179 and 241 cm^{-1} for the Raman active modes of Sb_4 in a neon matrix. These compare with the finite difference results in the present work (all modes) of 134, 174, and 235 cm^{-1}.

D. Trends in structures and other cluster properties

The structures of clusters of different group 15 elements show pronounced similarities, and appropriate scaling of the coordinates for one element is a reliable way of generating starting structures for another. The smallest clusters show a growth pattern based on the C_{2v} (butterfly) isomer of the tetramer, followed by a pattern of disordered pentagonal units for $n = 7$ and tube-like formation in the largest clusters considered here. Most atoms are threefold coordinated, and bond lengths close to the nearest-neighbor separation in the bulk (2.908 Å) are common. Two- and four-fold coordinated atoms have bonds that are shorter and longer, respectively, than this value. Bond angles in the range 80°–110° are common, but triangular structures and bond angles near 60° do not occur in the $A7$ structure of Sb ($\alpha \sim 95.5°$). Clusters studied here are clearly far from "bulklike."

The cohesive energies (Fig. 12) show very good agreement with available measured values ($n = 2, 3, 4$).[52] While there are signs of saturation with increasing n, the calculated value for Sb_{14} is lower than the experimental estimate of the bulk.[92] The odd-even variation with n is more pronounced than in group 16 elements sulfur[93] and tellurium[7] and is a direct consequence of the odd number of valence electrons in atoms of group 15 elements. The trends in cohesive energies are very similar to those found in Ref. 59. The DF/MD calculations of Sundararajan and Kumar[58] used the local density approximation for the exchange and correlation energies without spin corrections and led to large overestimates of the binding energies.

The overall similarity in the structures of clusters of group 15 elements does not imply that the relative energies of isomers

of a given cluster size are the same. The bonding in Sb and Bi clusters is weaker than in P clusters, and the range of isomer energies is smaller. The energy difference between isomers 8(a) and 8(g) in Fig. SF3 (supplementary material) is 0.47 eV in Bi and 0.67 eV in Sb, but over 1.7 eV in P. The $P_4(T_d)$-dimer is the most stable form of P_8, while in Bi and Sb it is ∼0.1 eV less stable than 8(a).

The vibration frequencies (Fig. SF6, supplementary material) cover the range of phonon frequencies measured in crystalline Sb (up to ∼73, 115–160 cm^{-1}).[87] Inelastic neutron scattering measurements on polycrystalline Sb[94] also show peaks around 60 and 150 cm^{-1},[94] and $q=0$ Raman spectra show vibrations at 154.6 cm^{-1} (A_{1g}, LO) and 116 cm^{-1} (E_g, TO).[95] Twofold coordinated atoms in the clusters have higher frequencies, and the $Sb_4(T_d)$-dimer frequencies are related to those of $Sb_4(T_d)$, supplemented by low-frequency vibrations corresponding to the weak bonds between the groups.

Relativistic effects[96] must be included in calculations involving heavy elements, and our scalar-relativistic pseudopotential for Sb includes the average of spin-orbit components, as in the case of Bi.[67] The stabilization of the $6p^3$ ($^4S^0_{3/2}$) atomic ground state by SOC is large in Bi, where the cohesive energies of Bi_n clusters are lowered almost uniformly by between 0.4 and 0.5 eV/atom,[67] but the effect of SOC in Sb_2 and Sb_4 is much weaker.[97] The VASP program[98] was used with the PBE functional, a projected augmented wave (PAW) pseudopotential for Sb with 15 valence electrons, and an energy cutoff of 500 eV. There is a significant lowering of total energy of the clusters and the constituent atoms, but the cohesive energies in the dimer and tetramers are changed by less than 0.1 eV/atom.

V. DISCUSSION AND CONCLUDING REMARKS

Combined density functional/molecular dynamics calculations have been performed on neutral Sb_n clusters ($n=2$–14) and on liquid Sb at 600, 700, 900, 1000, 1100, and 1300 K with 588 atoms in the simulation cell. They are the most extensive DF simulations performed to date on these systems, and we have focused on the structures and dynamical properties.

Antimony clusters show similar structural patterns (including coordination numbers, bond angles, ring patterns, ...) to those found in clusters of other group 15 elements. While these patterns are particularly evident in bulk allotropes of P, this is less so in Sb and Bi, where the most stable (rhombohedral) form is a modest distortion of a simple cubic structure comprising threefold coordinated atoms.[38,39] The energy differences between different isomers, and the energy barriers between them are less in Sb_n and Bi_n clusters than in the corresponding clusters of P and As. The structural patterns in the liquid and cluster phases of Sb and Bi are more similar to each other than to the crystalline $A7$ structures, and the structural variety in Sb clusters is reflected in the range of vibration frequencies up to ∼200 cm^{-1}. The power spectrum of the liquid shows a broad peak near 130 cm^{-1} at all temperatures, as well as a weaker peak near 40 cm^{-1} at lower temperatures.

Extensive elastic ND measurements have been performed on liquid Sb,[30] and the present calculations of the static structure factors $S(q)$ agree satisfactorily with these data. We are not aware of any inelastic scattering measurements of the dynamical structure factor $S(q,\omega)$, but our calculations of $S(q,\omega)$ and related quantities show clearly the presence of collective excitations. The low-q dispersion of these modes shows a sound velocity at 900 K of 2580 m/s, which is more than 20% higher than the adiabatic sound velocity measured at the melting point (1910,[28,90] 1884 m/s[29]). We would welcome experimental studies of these collective modes, as performed in Bi using inelastic ND[25] and x-ray scattering methods.[26]

The shear viscosity $\eta(q)$ has been determined from the transverse current correlation function $C_T(q,t)$, and the value of $\eta(0)$ has been determined by extrapolation $q \longrightarrow 0$. The result of the extrapolation depends on the number and distribution of q-points, but the viscosity decreases with increasing temperature in reasonable accord with the experiment. The Stokes-Einstein relationship between viscosity η and diffusivity D is satisfied to within 15%.

Monte Carlo calculations in liquid As[33] showed a strong preference for near-linear trimer structures with alternating short and long bonds. This feature is a possible marker of a Peierls distortion and is absent in the corresponding calculations of liquid Sb.[33] This finding is consistent with the contour plots of the angular limited bond-bond correlation function found in XAFS measurements[43] and in the present work (Fig. 13), which show few signs of alternating bonds at the melting point and above. The bond angle distributions (Fig. 4) show no preference for linear trimers, and they show

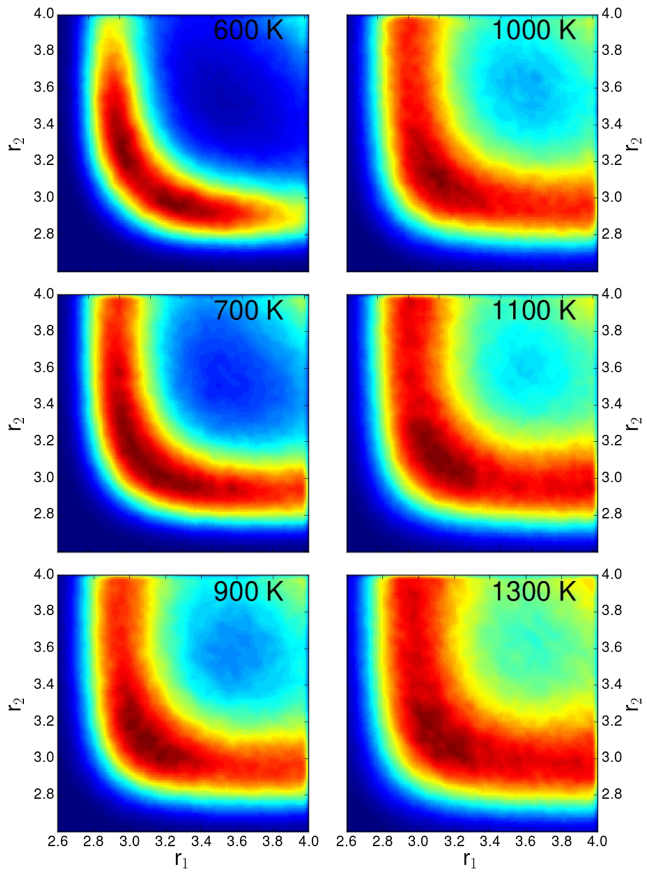

FIG. 13. Correlations between bond lengths r_1 and r_2 of three neighboring atoms with bond angle between 165° and 180°. The analysis covered the last 10 000 steps of each trajectory, and the cutoff for neighbors was 4.0 Å.

an *increase* in the relative number of 60° bond angles as the temperature increases. These distributions are consistent with the results of Fig. 13, and the deep minimum in the electronic DOS in crystalline Sb (Fig. 11) is absent. On the other hand, the supercooled liquid sample at 600 K shows both short-long bond alternation (two peaks in the correlation plot) and a pronounced minimum in the electronic DOS at the Fermi energy.

An alternative marker for a Peierls distortion is provided by Shor *et al.*,[22] who analyzed neutron scattering data for liquid Sb using a quasi-crystalline model of the structure. The analysis indicated that the short-range order is dominated by the $A7$ structure of the bulk at all temperatures. The focus is on details of the measured $S(q)$ function, particularly the asymmetry of the first peak and the form of the adjacent shoulder, that require a more accurate functional than PBE or PBEsol.

SUPPLEMENTARY MATERIAL

See supplementary material for plots of the ratio $S(q, E)/S(q)$ for selected values of q and temperature T of 600 K, 900 K, and 1300 K, as well as structures of Sb_n clusters for $5 \geq n \geq 14$, and vibration frequencies for selected cluster structures.

ACKNOWLEDGMENTS

We acknowledge gratefully the computer time provided by the JARA-HPC Vergabegremium on the JARA-HPC partition of the supercomputer JUQUEEN at Forschungszentrum Jülich and for time granted on the supercomputers JUROPA and JURECA at the Jülich Supercomputer Centre. We thank H. R. Schober for many helpful discussions, N. Atodiresei for performing calculations with spin-orbit coupling on Sb_2 and Sb_4, and G. Makov and colleagues for providing their original ND data. J.A. and M.R. acknowledge financial support from the Academy of Finland through its Centres of Excellence Program (Project No. 284621).

[1] J. Donohue, *The Structures of the Elements* (Wiley, New York, 1974), Chap. 8.
[2] J. C. Jamieson, Science **139**, 1291 (1963).
[3] D. Schiferl and C. S. Barrett, J. Appl. Crystallogr. **2**, 30 (1969).
[4] C. S. Barrett, P. Cucka, and K. Haefner, Acta Crystallogr. **16**, 451 (1963).
[5] P. Cucka and C. S. Barrett, Acta Crystallogr. **15**, 865 (1962).
[6] J. Akola, R. O. Jones, S. Kohara, T. Usuki, and E. Bychkov, Phys. Rev. B **81**, 094202 (2010).
[7] J. Akola and R. O. Jones, Phys. Rev. B **85**, 134103 (2012).
[8] C. Buzea and K. Robbie, Supercond. Sci. Technol. **18**, R1 (2004).
[9] Z. S. Popović, J. M. Kurdestany, and S. Satpathy, Phys. Rev. B **92**, 035135 (2015).
[10] S. Mardanya, V. K. Thakur, S. Bhowmick, and A. Agarwal, Phys. Rev. B **94**, 035423 (2016).
[11] O. Ü. Aktürk, V. O. Özçelik, and S. Ciraci, Phys. Rev. B **91**, 235446 (2015).
[12] A. Narayan, I. Rungger, and S. Sanvito, Phys. Rev. B **86**, 201402(R) (2012).
[13] H. Zhang, F. Freimuth, G. Bihlmayer, S. Blügel, and Y. Mokrousov, Phys. Rev. B **86**, 035104 (2012).
[14] J. K. Burdett and S. Lee, J. Solid State Chem. **44**, 415 (1982).
[15] X. Gonze, J.-P. Michenaud, and J.-P. Vigneron, Phys. Rev. B **41**, 11827 (1990).
[16] S. E. Boulfelfel, G. Seifert, Y. Grin, and S. Leoni, Phys. Rev. B **85**, 014110 (2012).
[17] Y. Katayama, T. Mizutani, W. Utsumi, O. Shinomura, M. Yamakata, and K. Funakoshi, Nature **403**, 170 (2000).
[18] G. Monaco, S. Falconi, W. A. Crichton, and M. Mezouar, Phys. Rev. Lett. **90**, 255701 (2003).
[19] Y. Tsuchiya, J. Phys.: Condens. Matter **9**, 10087 (1997).
[20] A. Chiba, M. Tomomasa, T. Higaki, T. Hayakawa, R. Takahashi, and K. Tsuji, J. Phys.: Conf. Ser. **121**, 022019 (2008).
[21] Y. Greenberg, E. Yahel, E. N. Caspi, C. Benmore, B. Beuneu, M. P. Dariel, and G. Makov, Europhys. Lett. **86**, 36004 (2009).
[22] Y. Shor, E. Yahel, and G. Makov, J. Non-Cryst. Solids **358**, 2687 (2012).
[23] H. J. Beister, K. Strössner, and K. Syassen, Phys. Rev. B **41**, 5535 (1990).
[24] K. Shibata, S. Hoshino, and H. Fujishita, J. Phys. Soc. Jpn. **53**, 899 (1984).
[25] L. Sani, L. E. Bove, C. Petrillo, and F. Sacchetti, J. Non-Cryst. Solids **353**, 3139 (2007).
[26] M. Inui, Y. Kajihara, S. Muneiri, S. Hosokawa, A. Chiba, K. Ohara, S. Tsutsui, and A. Q. R. Baron, Phys. Rev. B **92**, 054206 (2015).
[27] K. Lu, Q. Wang, C. Li, Y. Wang, and X. Chen, J. Non-Cryst. Solids **312-314**, 34 (2002).
[28] M. B. Gitis and I. G. Mikhailov, Sov. Phys. Acoust. **11**, 372 (1966).
[29] Y. Greenberg, E. Yahel, M. Ganor, R. Hevroni, I. Korover, M. P. Dariel, and G. Makov, J. Non-Cryst. Solids **354**, 4094 (2008).
[30] Y. Greenberg, E. Yahel, E. N. Caspi, B. Beuneu, M. P. Dariel, and G. Makov, Europhys. Lett. **133**, 094506 (2010).
[31] Y. Waseda and K. Suzuki, Phys. Status Solidi B **47**, 581 (1971).
[32] H. Kim, D. A. Boysen, J. M. Newhouse, B. L. Spatocco, B. Chung, P. J. Burke, D. J. Bradwell, K. Jiang, A. A. Tomaszowska, K. Wang, W. Wei, L. A Ortiz, S. A. Barriga, S. M. Poizeau, and D. R. Sadoway, Chem. Rev. **113**, 2075 (2012).
[33] C. Bichara, A. Pellegatti, and J.-P. Gaspard, Phys. Rev. B **47**, 5002 (1993).
[34] J. Hafner and W. Jank, Phys. Rev. B **45**, 2739 (1992).
[35] X.-P. Li, Phys. Rev. B **41**, 8392 (1990).
[36] K. Seifert, J. Hafner, and G. Kresse, J. Non-Cryst. Solids **205-207**, 871 (1996).
[37] J. Hegedus and S. R. Elliott, Phys. Status Solidi A **207**, 510 (2010).
[38] H. Jones, Proc. R. Soc. London, Ser. A **147**, 396 (1934).
[39] H. Jones, *The Theory of Brillouin Zones and Electronic States in Crystals* (Revised), 2nd ed. (North-Holland, Amsterdam, 1975), pp. 204–210.
[40] R. E. Peierls, *Quantum Theory of Solids* (Clarendon Press, Oxford, 1955), pp. 108–114.
[41] R. Bellisent, C. Bergman, R. Ceolin, and J. P. Gaspard, Phys. Rev. Lett. **59**, 661 (1987).
[42] M. Mayo, E. Yahel, Y. Greenberg, and G. Makov, J. Phys.: Condens. Matter **25**, 505102 (2013).
[43] Q. Wang, C. X. Li, Z. H. Wu, L. W. Wang, X. J. Niu, W. S. Yan, Y. N. Xie, S. Q. Wei, and K. Q. Lu, J. Chem. Phys. **128**, 224501 (2008).
[44] K. Sattler, J. Mühlbach, P. Pfau, and E. Recknagl, Phys. Lett. A **87**, 418 (1982).
[45] C. Bréchignac, P. Cahuzac, F. Carlier, M. de Frutos, J. Leygnier, and J. P. Roux, J. Chem. Phys. **102**, 763 (1994).
[46] T. M. Bernhardt, B. Kaiser, and K. Rademann, Phys. Chem. Chem. Phys. **4**, 1192 (2002).
[47] L. S. Wang, Y. T. Lee, D. A. Shirley, K. Balasubramanian, and P. Feng, J. Chem. Phys. **93**, 6310 (1990).
[48] M. L. Polak, G. Gerber, J. Ho, and W. C. Lineberger, J. Chem. Phys. **97**, 8990 (1992).
[49] M. Gausa, R. Kaschner, G. Seifert, J. H. Faehrmann, H. O. Lutz, and K.-H. Meiwes-Broer, J. Chem. Phys. **104**, 9719 (1996).
[50] H. Sontag and R. Weber, J. Mol. Spectrosc. **91**, 72 (1982).
[51] V. E. Bondybey, G. P. Schwartz, and J. E. Griffiths, J. Mol. Spectrosc. **89**, 328 (1981).
[52] J. Kordis and K. A. Gingerich, J. Chem. Phys. **58**, 5141 (1973).
[53] K. Balasubramanian and J. Li, J. Mol. Spectrosc. **135**, 169 (1989).
[54] K. K. Das, H. P. Liebermann, G. Hirsch, and R. J. Buenker, J. Chem. Phys. **102**, 8462 (1995).
[55] K. Balasubramanian, K. Sumathi, and D. Dai, J. Chem. Phys. **95**, 3494 (1991).
[56] H. Choi, C. Park, and K. K. Baeck, J. Phys. Chem. A **106**, 5177 (2002).
[57] H. Zhang and K. Balasubramanian, J. Chem. Phys. **97**, 3437 (1992).
[58] V. Sundararajan and V. Kumar, J. Chem. Phys. **102**, 9631 (1995).
[59] X. Zhao, J. Zhao, X. Chen, and W. Lu, Phys. Rev. A **72**, 053203 (2005).
[60] R. O. Jones and D. Hohl, J. Chem. Phys. **92**, 6710 (1992).
[61] R. O. Jones and G. Seifert, J. Chem. Phys. **96**, 7564 (1992).
[62] P. Ballone and R. O. Jones, J. Chem. Phys. **100**, 4941 (1994).
[63] J. P. Perdew, Phys. Rev. B **33**, 8822 (1986); A. D. Becke, Phys. Rev. A **38**, 3098 (1988).
[64] D. Hohl and R. O. Jones, Phys. Rev. B **50**, 17047 (1994).

[65]R. O. Jones, Rev. Mod. Phys. **87**, 897 (2015).
[66]P. Ballone and R. O. Jones, J. Chem. Phys. **121**, 8147 (2004).
[67]J. Akola, N. Atodiresei, J. Kalikka, J. Larrucea, and R. O. Jones, J. Chem. Phys. **141**, 194503 (2014).
[68]M. Ropo, J. Akola, and R. O. Jones, J. Chem. Phys. **145**, 184502 (2016).
[69]M. Ropo, J. Akola, and R. O. Jones (unpublished).
[70]CPMD V3.15 © IBM Corp. 1990-2011, © MPI für Festkörperforschung Stuttgart 1997-2001, http://www.cpmd.org.
[71]N. Troullier and J. L. Martins, Phys. Rev. B **43**, 1993 (1991).
[72]J. P. Perdew, K. Burke, and M. Ernzerhof, Phys. Rev. Lett. **77**, 3865 (1996).
[73]S. G. Louie, S. Froyen, and M. L. Cohen, Phys. Rev. B **26**, 1738 (1982).
[74]J. P. Perdew, A. Ruzsinszky, G. I. Csonka, O. A. Vydrov, G. E. Scuseria, L. A. Constantin, X. Zhou, and K. Burke, Phys. Rev. Lett. **100**, 136406 (2008).
[75]J. Tao, J. P. Perdew, V. N. Staroverov, and G. E. Scuseria, Phys. Rev. Lett. **91**, 146401 (2003).
[76]M. Micoulaut, J. Chem. Phys. **138**, 061103 (2013).
[77]S. Grimme, J. Comput. Chem. **27**, 1787 (2003).
[78]M. J. Assael, A. E. Kalyva, K. D. Antoniadis, R. M. Banish, I. Egry, J. Wu, E. Kaschnitz, and W. A. Wakeham, High Temp. - High Pressures **41**, 161 (2012).
[79]S. Le Roux and V. Petkov,"ISAACS: Interactive structure analysis of amorphous and crystalline systems," J. Appl. Crystallogr. **43**, 181 (2010).
[80]I. Heimbach, F. Rhiem, F. Beule, D. Knodt, J. Heinen, and R. O. Jones, J. Comput. Chem. **38**, 389 (2017).
[81]W. E. Alley and B. J. Alder, Phys. Rev. A **27**, 3158 (1983).
[82]A. Einstein, Ann. Phys. **322**, 549 (1905).
[83]U. Balucani, R. Vallauri, and T. Gaskell, Phys. Rev. A **35**, 4263 (1987).
[84]G. Makov, personal communication (2016).
[85]J. L. F. Da Silva, J. Appl. Phys. **109**, 023502 (2011).
[86]T. Matsunaga, J. Akola, S. Kohara, T. Honma, K. Kobayashi, E. Ikenaga, R. O. Jones, N. Yamada, M. Takata, and R. Kojima, Nat. Mater. **10**, 129 (2011).
[87]R. I. Sharp and E. Warming, J. Phys. F: Met. Phys. **1**, 570 (1971).
[88]S. T. Lin, M. Blanco, and W. A. Goddard, J. Chem. Phys. **119**, 11792 (2003).
[89]P. Lamparter and S. Steeb, Z. Naturforsch. A **32**, 1021 (1977).
[90]S. Blairs, Int. Mater. Rev. **52**, 321 (2007).
[91]X. Gonze, J.-P. Michenaud, and J.-P. Vigneron, Phys. Scr. **37**, 785 (1987).
[92]R. Hultgren, P. D. Desai, D. T. Hawkins, M. Gleiser, K. K. Kelley, and D. G. Wagman, *Selected Values of the Thermodynamic Properties of the Elements* (American Society for Metals, Metals Park, OH, 1973), p. 445.
[93]R. O. Jones and P. Ballone, J. Chem. Phys. **118**, 9257 (2003).
[94]J. Salgado, Ber. Kernforschungszentrum Karlsruhe KFK 1954, Karlsruhe, Germany, 1974; H. R. Schober and P. H. Dederichs, "Phonon states of elements. Electron states and Fermi surfaces of alloys. Sb: Datasheet," in *Phonon States of Elements. Electron States and Fermi Surfaces of Alloys*, Landolt-Börnstein - Group III Condensed Matter, edited by K.-H. Hellwege and J. L. Olsen (Springer-Verlag, Berlin, Heidelberg, 1981), Vol. 13A.
[95]J. Höhne, U. Wenning, H. Schulz, and S. Hüfner, Z. Phys. B **27**, 297 (1977).
[96]K. Balasubramanian and K. S. Pitzer, in *Ab Initio Methods in Quantum Chemistry. I*, Advances in Chemical Physics Vol. 67, edited by K. P. Lawley (Wiley, New York, 1987), p. 287.
[97]N. Atodiresei, personal communication (2016).
[98]G. Kresse and J. Furthmüller, Phys. Rev. B **54**, 11169 (1996).